

Polarization properties of solid-state organic lasersI. Gozhyk,^{1,*} G. Clavier,² R. Méallet-Renault,² M. Dvorko,² R. Pansu,² J.-F. Audibert,² A. Brosseau,² C. Lafargue,¹ V. Tsvirkun,¹ S. Lozenko,¹ S. Forget,³ S. Chénais,³ C. Ulysse,⁴ J. Zyss,¹ and M. Lebalat¹¹*Laboratoire de Photonique Quantique et Moléculaire, CNRS UMR 8537, Institut d'Alembert FR 3242, Ecole Normale Supérieure de Cachan, 61 Avenue du Président Wilson, F-94235 Cachan, France*²*Laboratoire de Photophysique et Photochimie Supramoléculaires et Macromoléculaires, CNRS UMR 8531, Institut d'Alembert FR 3242, Ecole Normale Supérieure de Cachan, F-94235 Cachan, France*³*Université Paris 13, Sorbonne Paris Cité, Laboratoire de Physique des Lasers, CNRS UMR 7538, F-93430, Villetaneuse, France*⁴*Laboratoire de Photonique et Nanostructures, CNRS UPR20, Route de Nozay, F-91460 Marcoussis, France*

(Received 24 July 2012; published 12 October 2012)

The polarization states of lasers are crucial issues both for practical applications and fundamental research. In general, they depend in a combined manner on the properties of the gain material and on the structure of the electromagnetic modes. In this paper, we address this issue in the case of solid-state organic lasers, a technology which enables one to vary independently gain and mode properties. Different kinds of resonators are investigated: in-plane microresonators with Fabry-Perot, square, pentagon, stadium, disk, and kite shapes, and external vertical resonators. The degree of polarization P is measured in each case. It is shown that although transverse electric modes prevail generally ($P > 0$), the kite-shaped microlaser generates negative values for P (i.e., a flip of the dominant polarization which becomes mostly transverse magnetic polarized). In general, we demonstrate that both the pump polarization and the resonator geometry can be used to tailor the polarization of organic lasers. With this aim in view, we, at last, investigate two other degrees of freedom, namely upon using resonant energy transfer and upon pumping the laser dye to a higher excited state. We then demonstrate that significantly lower P factors can be obtained.

DOI: [10.1103/PhysRevA.86.043817](https://doi.org/10.1103/PhysRevA.86.043817)

PACS number(s): 42.55.Sa, 42.55.Mv, 42.60.Da, 05.45.Mt

I. INTRODUCTION

Light-matter coupling issues are firmly based on quantum electrodynamics foundations. However, practical consequences on real systems are often difficult to derive due to sometimes complicated quantum formulations. Maxwell-Bloch equations provide a semiclassical expression more appropriate for lasers [1], which are usually macro- or mesoscopic systems. The resulting nonlinear coupled equations could be handled by means of numerical simulations, which nevertheless face major problems for large systems due to huge meshes. This obstacle is even increased when polarization states of electromagnetic modes are involved, since they require the treatment of three-dimensional and vectorial Maxwell equations. And yet, polarization remains a key point for many photonics components.

We would like to address this issue by way of micron- and millimeter-sized lasers of various resonator geometries, which are out of reach of full electromagnetic simulations due to their large scale, but where validity of the semiclassical (or geometrical optics) limit is expected to provide a simplified insight [2]. In this work, we propose to evidence and analyze polarization effects in solid-state organic laser systems, and demonstrate the possibility to modify the output polarization by playing on cavity shape or on material related features.

Previous works have been devoted to microresonators of circular geometry [3–5], coated fibers [6,7], and distributed feedback lasers (see, for instance, [8]). In this work, we focus on vertical emitting devices [vertical external cavity surface emitting organic lasers (VECSOLs) [9]], where the

properties of the gain material can be quite easily decoupled from the cavity shape, and on thin-film planar microlasers of various contours, such as square, pentagon, kite, etc. Actually planar microresonators have become widely used in photonics systems, from integrated optics [10] to fundamental physics (see, for instance, [11] or [12]). But in general, their use is limited to Fabry-Perot (i.e., the resonance occurs between flat parallel edges) or circular shapes, namely spheres, disks, rings, or tori, while a great variety of geometries (polygons, stadium, etc.) can be easily fabricated with nanometric etching quality, providing specific advantages, such as a higher directivity of emission [13,14], a better coupling to waveguides [15], or a high stability of modes versus perturbations [16]. The studies of these geometrical features remain to be improved—in particular when the polarization of modes is involved—and should lead to optimized devices for both fundamental and applied photonics. In particular, we will show hereafter that in-plane polarization is in general favored by gain and propagation, whereas out-of-plane polarization could be of crucial importance for applications, like sensing [17], for instance. We will then propose different ways to monitor the ratio of polarizations, making use either of the gain or of the resonator shape.

The experiments were carried out with solid-state organic lasers [18]. Their interest for this study is twofold. First, organic technology ensures a high etching quality from a relatively fast and easy fabrication, which enables one to investigate a great variety of resonator shapes. Secondly, the flexibility of organic chemistry allows one to explore various gain media in different pumping schemes in order to monitor the polarization states, as demonstrated in Secs. VI and VII. The analysis of the experimental results is then performed in the framework of “polarization spectroscopy,” a domain

*igozhyk@lpqm.ens-cachan.fr

specific to organic materials, which matured in the late 1980s and has given birth to various applications in polymer physics or biology (see [19] and [20] for a review). This domain is based on the fluorescence anisotropy of dye molecules. A few theoretical articles [21–23] extend its range to the nonlinear regime of stimulated emission and lasers, as it was soon evidenced that unlike most other solid-state laser media, the output polarization of a solid-state dye laser does not only depend on the anisotropy of the gain medium or on the polarization-dependant losses due to the cavity, but also depends on the pump beam polarization [21,22]. The objective of this paper is to better understand the polarization characteristics of planar organic microresonators, in order to tailor the polarization output of these devices.

The paper is organized as follows. The experimental configurations are described in Sec. II. Basics on fluorescence anisotropy are then recalled in Sec. III, a more detailed analysis being postponed to the appendixes. The specific case of amplified spontaneous emission (ASE) is dealt with in Sec. IV. Then polarizations of laser modes are reported and discussed for various cavity shapes in Sec. V. These results evidence a strong influence of the polarization of the pump beam as expected, which prevents populating numerous families of modes, that would be otherwise available. In order to release this constraint and improve the accessibility of modes, we propose and demonstrate two different methods to tailor the polarization of the emission: on the one hand, a nonradiative energy transfer from an excited molecule to the dye laser (Sec. VI) and, on the other hand, the direct pumping to a higher excited state of the dye molecule (Sec. VII).

II. EXPERIMENTAL SETUPS

In this paper, we consider thin-film-based lasers in two different configurations represented in Fig. 1. The gain layer is made of a spin-coated poly(methylmethacrylate) (PMMA)

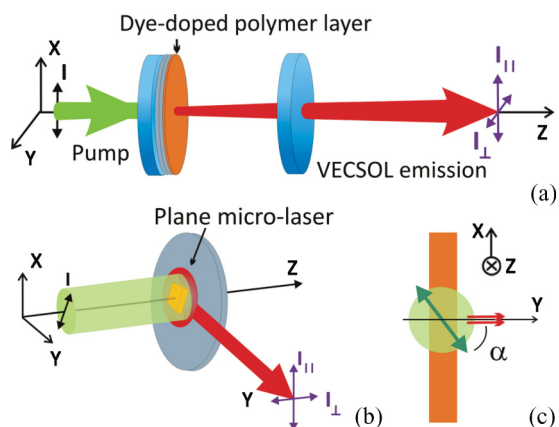


FIG. 1. (Color online) Experimental configurations of the solid-state organic lasers: (a) vertical emission (VECSOL) and (b) planar microlaser (oblique view); (c) planar microlaser geometry from a top view (xy plane), indicating the α angle between the polarization of the pump beam and the direction of observation (y), illustrated with the case of a Fabry-Perot cavity. For (a)–(c) the colors are green for pumping and red for emission.

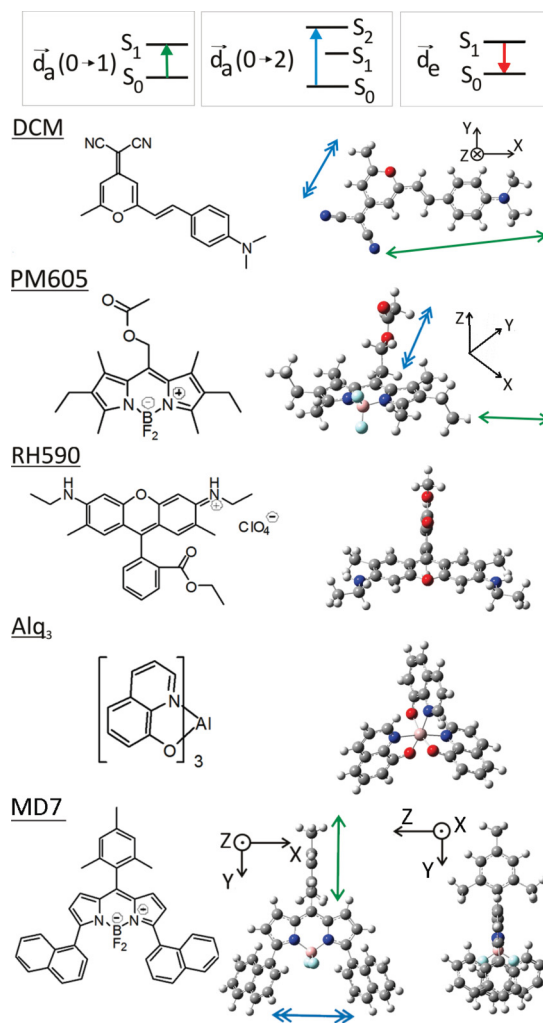


FIG. 2. (Color online) The molecular energy levels involved in the transitions are schematically shown on the top of the figure. Dye molecules involved in the study are as follows: DCM, PM605, RH590, Alq₃, and MD7. MD7 is a homemade modified pyromethene. For DCM, PM605, and MD7 the calculated absorption transition dipoles are indicated with a single arrow for the $S_0 \rightarrow S_1$ transition and with a double arrow for the $S_0 \rightarrow S_2$ transition. For PM605, two transitions with similar oscillator strengths are involved when pumped at 355 nm. One of the absorption dipoles is parallel to the absorption dipole of the $S_0 \rightarrow S_1$ transition and is thus not represented.

film doped with laser dyes,¹ which are either commercial molecules, namely DCM, pyromethene 605 (PM605), and rhodamine 590 (RH590), or noncommercial dye like MD7 [24]. To optimize the lasing efficiency, the concentration is typically 5% wt for in-plane microlasers and 1% wt for VECSOL, and the layer thickness is $0.6 \mu\text{m}$ and $20 \mu\text{m}$, respectively. In case of VECSOL, the substrate is directly the back mirror of the cavity, while for in-plane microresonators it is a commercial silicon wafer with a $2\text{-}\mu\text{m}$ silica buffer layer.

¹In this paper, each commercial dye was bought from Exciton, and PMMA from MicroChem, 6% wt in anisole 495 000 average chain length for in-plane microlasers and 15% wt 950 000 for VECSOL.

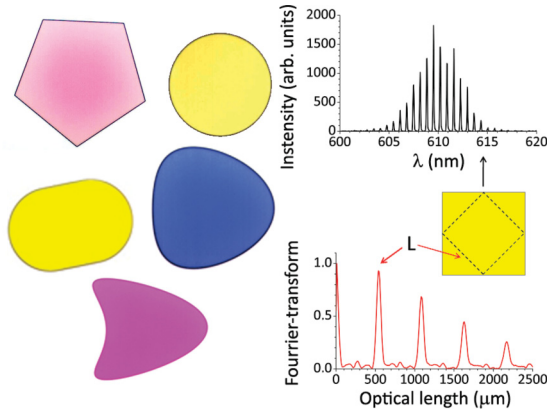


FIG. 3. (Color online) (a) Optical microscope photos of planar microlasers, which are investigated in this paper. Scales are $0.6 \mu\text{m}$ for the thickness and about $100 \mu\text{m}$ in-plane. Colors depend on the dye molecules. (b) Typical experimental spectrum of a square microlaser. (c) Fourier transform of the spectrum in (b). The position of the first peak indicates the optical length L of the periodic orbit (i.e., diamond) drawn in the inset, according to the data process described in [26].

The specificities of each device are depicted in Fig. 1. In VECSOL [Fig. 1(a)], the cavity feedback is ensured by a curved dielectric mirror [9]. The pump beam radius is matched to the fundamental TEM₀₀ cavity mode, which is much smaller than the diameter of the mirrors. So we assume a rotational symmetry of the setup, which is only broken by the polarization of the pump beam. In this sense, this geometry enables studying the sole influence of lasing gain medium on polarization, irrespective of any cavity-related effect. On the contrary, it is the geometries of the in-plane microlasers [Fig. 1(b)] which determines the types of modes which are lasing. Such cavities are fabricated from the single gain layer by electron-beam lithography, which ensures nanometric etching quality [25]. Arbitrary cavity contours can be designed [see Fig. 3(a)] to act as resonators. The emission of a single cavity is then collected in its plane.

Both types of devices are pumped with a pulsed linearly polarized frequency-doubled Nd:YAG laser (532 nm, 500 ps, 10 Hz). The emission is injected via a fiber to a spectrometer connected to a cooled CCD camera, allowing one to infer the lasing modes from their spectrum [see Figs. 3(b) and 3(c)] [26]. A polarizer is set between the device under study and the fiber to project the electric field of the far-field emitted beam onto two orthogonal directions, called I_{\parallel} and I_{\perp} (see Fig. 1).

The VECSOL configuration is close to the usual geometry in fluorescence anisotropy measurements, since I_{\parallel} is registered in the direction parallel to the pump polarization and I_{\perp} in the orthogonal direction. On the contrary, the case of in-plane microlasers is quite different. Actually the pump beam propagates perpendicularly to the cavity plane and its size is much larger than a single cavity, so that the pump intensity may be considered constant over one resonator. Thus although the polarization of the pump beam always lies within the cavity plane, the emission may be collected along any line within the cavity plane, which means that I_{\parallel} is not always parallel to the pump polarization. However, we uniformize the terminology for the two configurations by calling I_{\parallel} and I_{\perp} as well, the components polarized within (I_{\parallel}) and perpendicularly (I_{\perp}) to

the film plane [Fig. 1(b)]. In order to describe the orientation of the pump polarization within the cavity plane, we also introduce the angle α defined as the angle between the pump polarization and the direction of observation [see Fig. 1(c)].

III. BASICS IN EMISSION ANISOTROPY

Before investigating stimulated emission in the following sections, we first review a few basic features in fluorescence anisotropy in connection with our specific solid-state systems.

An isotropic ensemble of dye molecules is known to emit light with a nontrivial polarization state. This phenomenon is known as fluorescence anisotropy and has generated a broad literature (see [19] and [20] for a review). If the pump laser is linearly polarized, then the fluorescence emission is not *a priori* equally polarized along the directions parallel I_{\parallel} and perpendicular I_{\perp} to the polarization of the pump (see Fig. 1 for notations). This anisotropy can be quantified by the degree of polarization²:

$$P = \frac{I_{\parallel} - I_{\perp}}{I_{\parallel} + I_{\perp}},$$

which is zero for equal polarizations, and otherwise remains between -1 and 1 from a mathematical point of view. However its range is restricted due to physical limitations as discussed later in this section.

In experiments, the overall inaccuracy can be estimated to less than 0.05 unit for P . The P value can be inferred after integration over the whole spectrum for each polarization or by considering a specific mode, both methods leading to almost the same value if a single mode family is involved.

In a liquid solution, the dye molecules are free to rotate. The degree of polarization P is then zero, except at short delays after the excitation pulse. Once doped into a rigid polymer matrix, like PMMA, the fluorophores are not yet able to move, either by thermal or Weigert effects [27,28], and P could then be nonzero even under a stationary pumping. However if the dye concentration is high enough, Förster resonant energy transfer (RET) occurs between nearby molecules and tends to isotropize the emitted fluorescence under continuous excitation [29]. However, we noticed that RET is no longer a limitation to the emission anisotropy in the case of stimulated emission. This observation could be explained by the difference of time scales, which is of the order of the fluorescence lifetime (i.e., nanoseconds) for RET [19,20] and could be as short as a few picoseconds for stimulated emission [30,31]. In this paper, we consider various dye molecules doped in a rigid PMMA matrix in a stimulated emission regime. We then assume that the fluorophores are not rotating and moreover that RET does not occur between laser dye molecules under subnanosecond pumping conditions.

To deal with lasing, a full nonlinear approach should be derived. Some models were already developed [21–23], but as a robust theory is not yet mature, we prefer to resort here

²Sometimes, the anisotropy parameter $r = (I_{\parallel} - I_{\perp}) / (I_{\parallel} + 2I_{\perp})$ is used. But in our experiments, no longitudinal component of the electric field is expected in the far field, so the normalized factor is $I_{\parallel} + I_{\perp}$ and not $I_{\parallel} + 2I_{\perp}$.

to a phenomenological approach. We assume that the dye molecules can be modeled as independent emitters, and only consider the influence of the geometry of the laser cavity. We will show hereafter that in general this simplified approach is able to capture the main physical features.

The sample is supposed to be exposed to a linearly polarized light. The probability that a dye molecule absorbs the pump light is proportional to $\cos^2(\chi)$, where χ is the angle between the pump polarization and the absorption transition dipole \vec{d}_a of the molecule. Then the emission of the molecule is assumed to be that of an emitting transition dipole \vec{d}_e in the far field. The dipoles \vec{d}_a and \vec{d}_e depend on the transitions which are involved in the absorption and subsequent emission processes. In this paper, we will consider the electronic transitions $S_0 \rightarrow S_1$ and $S_0 \rightarrow S_2$ for absorption, and $S_1 \rightarrow S_0$ for emission (see Fig. 2). Each electronic level S_i is broadened by vibrations, which allows one to consider dye molecules as an effective four-level laser system [32]. In general, there is an angle β between \vec{d}_a and \vec{d}_e , which depends on the molecular structure. A more detailed account is given in Appendix A and some \vec{d}_a were calculated with GAUSSIAN software and reported in Fig. 2.

The total electric field is then obtained from the integration over the orientations of the fluorophores. The distribution of these orientations is not *a priori* isotropic due to polymer stress [33] during spin coating, as it was reported for π conjugated polymers [34,35]. However, it was observed that PMMA does not present an alignment due to spin coating [36] and that the dye molecules embedded into PMMA remain isotropically distributed [37].³ Hence we only consider an isotropic distribution of dye molecules. The case of an anisotropic distribution of dyes is theoretically addressed elsewhere [38], and checked experimentally in [31].

The analytical calculation of P in both configurations is detailed in Appendix B. For the VEC SOL case, according to our model, P depends only on the angle β between the absorption and emission transition moments of the dye molecule:

$$P_{\text{VECSOL}} = \frac{3 \cos^2 \beta - 1}{3 + \cos^2 \beta}. \quad (1)$$

For the in-plane geometry, P depends also on the angle α of the pump polarization within the gain layer, and on the specific resonance which is excited. For the bulk case, we show in Appendix B that the expression of P is the following:

$$P_{\text{in plane}} = \frac{(3 \cos^2 \beta - 1)(1 - \cos 2\alpha)}{7 - \cos^2 \beta - \cos 2\alpha(3 \cos^2 \beta - 1)}. \quad (2)$$

It is plotted versus the angle β in Fig. 4 for various angles α . The degrees of polarization P in the in-plane and VEC SOL configurations are then not equal, except for $\alpha = \pi/2$. However, the general meaning is similar and the calculations detailed in Appendix B lead to similar conclusions for both: I_{\perp}

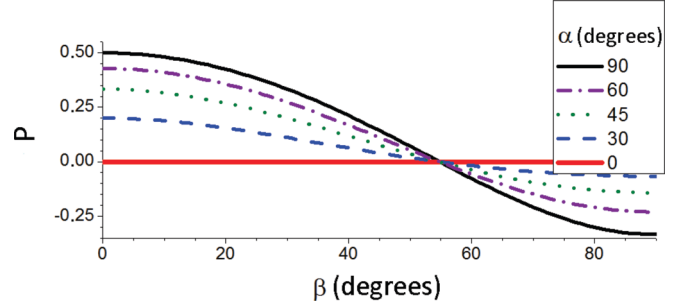


FIG. 4. (Color online) Degree of polarization $P_{\text{in plane}}$ versus the angle β between the absorption and emission dipoles, following expression (2). For $\alpha = \pi/2$, $P_{\text{in plane}} = P_{\text{VECSOL}}$.

does not depend on the orientation of the pump polarization α , and gets maximum (and P minimum) when $\beta \rightarrow \pi/2$. The practical case of stimulated emission in specific resonator geometries is developed in the following sections.

IV. AMPLIFIED SPONTANEOUS EMISSION (IN PLANAR CONFIGURATION)

The emission anisotropy is jointly determined by the molecular properties and the electromagnetic modes which sustain the generated light. This section deals with amplified spontaneous emission (ASE), which involves the nonlinear process of stimulated emission, but does not depend on the actual resonator shape. In ASE conditions, the emission is spontaneously generated within the excited gain medium and amplified by a single path propagation without any feedback.

ASE experiments were carried out in the in-plane configuration, but without any cavity shaping. A usual DCM-PMMA layer was pumped prior to any etching and the emission collected in-plane as described in Sec. II. Figure 5 (circles) shows, however, that P is always higher than the value expected from the fluorescence model ($P < 0.5$ for any angle β as seen in Fig. 4), and increases with the pump intensity [39].⁴ Actually the anisotropy value defined from a fluorescence process in the previous section represents the anisotropy well below the ASE threshold, whenever spontaneous emission is dominant over stimulated emission. This fluorescence is mainly polarized in plane, since the pump polarization lies within the plane, and so the dyes oriented such as \vec{d}_a lying in-plane are predominantly excited. And as β is small in general for an S_0 - S_1 transition, they predominantly emit in-plane. As the ASE is fed by spontaneous photons that have a dominant polarization, the excited molecules are prone to mostly emit photons with this given polarization. Thus the avalanche effect amplifies the difference between the polarized components, I_{\parallel} is favored [8], and then P increases with the pump intensity.

The previous discussion summons up the properties of the dye molecules to explain the prevalence of I_{\parallel} over I_{\perp} . Furthermore, even in the absence of cavity, photons propagate within specific electromagnetic modes, which also tends to

³The molecular weight of the PMMA used in [36] is 15 000, while it is 495 000 in our experiments. It is not specified in [37]. This parameter could be relevant for the organization of the layer by spin-coating. The case of an anisotropic distribution of fluorophores was theoretically dealt with in [38].

⁴At low pump intensities, the ASE data are not shown on Fig. 5 due to low output intensity and thus high experimental uncertainties.

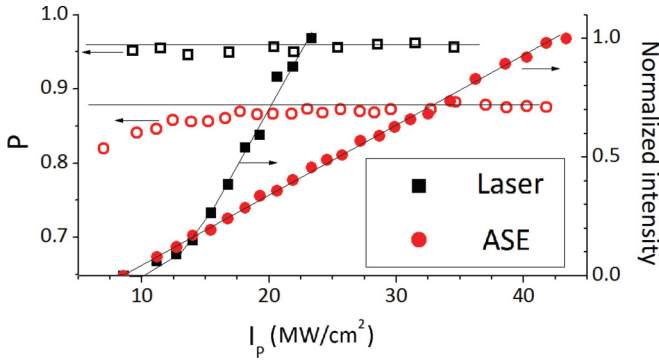


FIG. 5. (Color online) Degree of polarization P versus the pump intensity I_p (per pulse) for ASE and Fabry-Perot in planar microresonator configuration for a DCM-PMMA layer. The intensity of emission versus I_p is presented for comparison. Thin lines are drawn for guiding eyes.

enhance I_{\parallel} . Therefore, in order to get a more comprehensive interpretation, an analysis of the modes must be performed.

In such in-plane configuration with infinite layers, the approximation of the effective refractive index applies. The electromagnetic field can then be split into two independent sets of modes with independent polarizations, traditionally labeled transverse electric (TE) [respectively, transverse magnetic (TM)] if there is no electric (respectively, magnetic) component along the z direction (see Fig. 6). It must be pointed out that, as the polarizer used for analysis is selective on the electric field, a measure of I_{\perp} is sensitive only to TM modes (E_z component), while I_{\parallel} should *a priori* gather both TE and TM mode contributions (E_x component; see Fig. 6). In the case of ASE experiments with infinite layers, the electric field of the TM mode is measured in the far field and is thus purely polarized along the z direction (i.e., no E_x component). The strict equivalence TE- I_{\parallel} and TM- I_{\perp} is then valid.

The parameters of our samples are gathered in Fig. 6. The bulk refractive index of PMMA is 1.49 at 600 nm and increased slightly with the addition of a dye, for instance, $n = 1.54$ for 5% wt DCM in PMMA. Assuming an infinite silica layer, then there exists a single mode for each polarization (one TE and one TM) propagating inside the doped PMMA layer, both with close effective refractive index, $n_{\text{eff}} \simeq 1.50$. However the tiny differences are enhanced by the nonlinearity of stimulated emission. First, the effective index of TE is slightly higher than that of TM ($\Delta n \simeq 5 \times 10^{-3}$), which means that the TE mode is more localized inside the gain layer [40] and thus

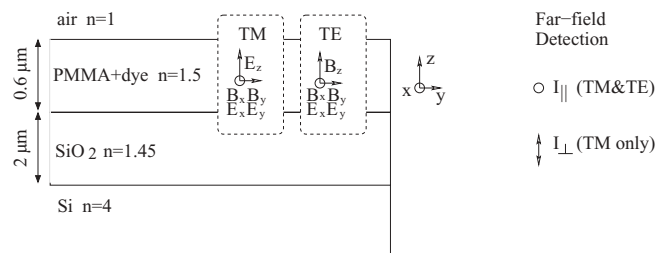


FIG. 6. Scheme of a sample slice in in-plane configuration (not at scale), with approximative values of bulk refractive indexes at 600 nm.

more amplified. Secondly, the silica layer is finite. Losses through the silicon layer are then altering mostly the TM mode, which is less confined into the PMMA propagating layer. These arguments show that mode considerations (without molecular influence) can explain the discrepancy between both components.

So even for ASE, which is the simplest case involving stimulated emission, both molecular properties and mode propagation combine to enhance I_{\parallel} , whatever is the dye laser. At low pump intensity, $P_{\text{DCM}} = 0.8$ and $P_{\text{PM605}} = 0.65$. Both P are higher than 0.5, which is the maximal value expected for an ensemble of isotropically fluorescent dipoles, for any β . In the general case of an arbitrary shape of resonator, the effective index approximation fails at the boundary (since the layers are not infinite) [41], and the measure of P may provide an insight into the electromagnetic modes which coexist within the cavity as will be considered in the next section.

V. INFLUENCE OF THE CAVITY SHAPE

The resonator modifies the degree of polarization in two different ways. It creates a feedback which enhances further the dominant component (i.e., I_{\parallel}). But at the same time, for in-plane microcavities, reflections at the boundary couple components of the electromagnetic field and lead to a partial redistribution of the energy.

The simplest case to consider is the Fabry-Perot cavity (i.e., the classical two-mirrors cavity), in which polarization states have been extensively studied with liquid dye lasers (see, for instance, [42–44]), but more rarely in the solid state [39,45].

I. VECOLS

In VEC SOL configuration with a RH640-PMMA layer, the degree of polarization P equals to unity for a linearly polarized pump beam, which means that the lasing emission is totally polarized, like the pump. Moreover when the pump beam is circularly polarized, the lasing emission is not polarized, which means that there is no noticeable difference between the I_{\parallel} and I_{\perp} components, and a quarter wave plate added on the beam path does not allow to recover a preferential polarization direction. These results were recorded for a 1-cm-long cavity and above threshold. According to Refs. [39,44,46,47], cavity length and pump intensity should be relevant parameters, since they monitor the build-up time of the modes [48]. Work is in progress to get a more comprehensive understanding of the polarization states in this simple geometry which is rotational invariant [axis z ; see Fig. 1(a)].

Another experiment was carried out with a (5% wt) DCM-PMMA layer, inserting a glass plate inside the cavity at Brewster angle to force the emission polarization, and then turning the polarization of the pump beam by a variable angle α' (see inset of Fig. 7 for notation). The laser threshold for $\alpha' = \pi/2$ was found twice higher than for $\alpha' = 0$. Then the pump intensity is fixed just above the higher threshold and the emitted intensity is recorded versus α' . The results are summarized with squares in Fig. 7 and show strong modulations. The curve in Fig. 7 was inferred from the calculations presented in Appendix B. Actually, the geometry of this system is similar to that of the in-plane configuration with $\alpha = \alpha'$. In the case of fluorescence, the emitted intensity

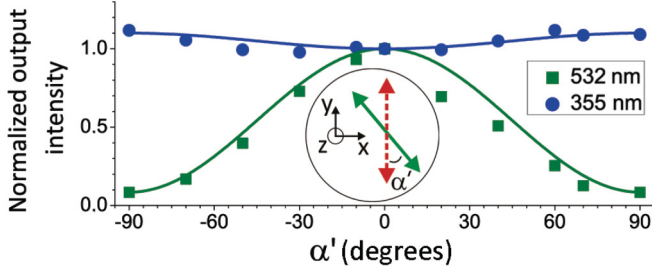


FIG. 7. (Color online) Normalized intensity emitted from a VECSOL with a PMMA-DCM gain material, versus the angle α' of the pump polarization. Comparison between a 532-nm pump (green, squares) and a 355-nm pump (blue, circles), after corrections from bleaching. The curves are fitted according to Eq. (3). (Inset) Scheme of a VECSOL section. The polarization of emission is fixed and represented as a dotted red arrow, while the linear pump polarization is shown as a green continuous arrow.

should then be predicted by Eq. (B3), which is a linear function of $\cos 2\alpha'$. So,

$$\frac{I(\alpha')}{I(\alpha' = 0)} = A + B \cos 2\alpha', \quad (3)$$

where $\frac{A}{B} = \frac{3 + \cos^2 \beta}{1 - 3 \cos^2 \beta}$. Equation (3) is plotted in Fig. 7 up to a scale parameter and shows a good agreement with experiments, which indicates that the VECSOL is working not far from a linear regime, since Eq. (3) is inferred from fluorescence predictions.

2. Planar microlasers

In the case of the in-plane configuration, the symmetry is naturally broken between I_{\parallel} and I_{\perp} . Actually TE and TM polarizations experience slightly different losses during propagation, as mentioned in the previous section. Moreover, their reflection coefficients at the microresonator boundaries could be different, even at normal incidence, due to the thinness of the layer [49]. In any case, P is recorded at a higher level

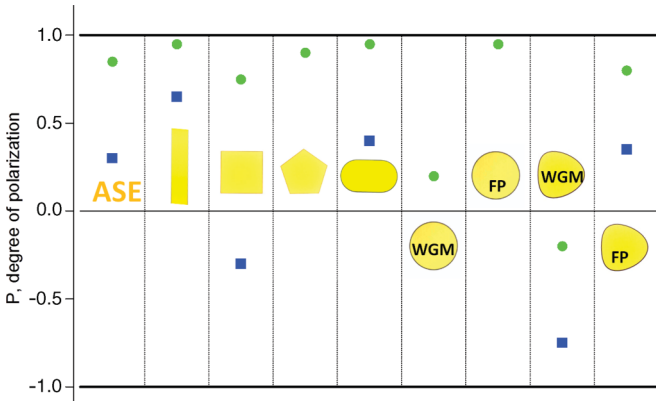


FIG. 8. (Color online) Degree of polarization P in connection with the resonator shape for a DCM-PMMA layer pumped at 532 nm (green disks) and a MD7-PMMA layer pumped at 355 nm (blue squares). (From left to right) ASE, Fabry-Perot, square (diamond modes), pentagon (inscribed pentagon), stadium (WGM), disk (WGM), disk (Fabry-Perot modes), kite (WGM), and kite (Fabry-Perot modes).

TABLE I. Comparison of P obtained from ASE and various shapes of microlasers in the in-plane configuration, depending on the dye laser and the wavelength of excitation. Some cavity shapes (e.g., disk and pentagon) were not available for each laser dye presented in this table. Moreover lasing under the UV pump was not achieved systematically for each shape.

P	532 nm			355 nm		
	DCM	PM605	MD7	DCM	DCM-Alq ₃	MD7
ASE	0.85	0.65	0.6	0.1	0.05	0.3
Fabry-Perot	0.95	0.95	0.9	0.9	0.9	0.65
Square	0.75	0.85	0.7	0.7	0.55	-0.3
Pentagon	0.9	0.95	-	-	-	-
Stadium	0.95	0.85	0.1	0.5	0.4	0.4
Disk (FP modes)	0.95	0.87	-	0.5	-	-
Disk (WGM)	0.2	-	-	-	-	-
Kite (FP modes)	0.8	0.7	0.9	-	-	0.35
Kite (WGM)	-0.2	-0.85	-0.7	-0.54	-0.55	-0.75

than in ASE experiments, which indicates that laser feedback further enhances the prevalent polarization. P depends neither on the specific dye molecule used ($P_{\text{DCM}} = P_{\text{PM650}} = 0.95$), nor on the pump intensity (see Fig. 5), nor on the cavity length (checked from 100 to 200 μm). These observations could be accounted for by a short building time and short photon lifetime (~ 1 ps), compared to the fluorescence lifetime (~ 1 ns).

In the in-plane microlaser configuration, the degree of polarization P was measured for various cavity shapes and the results gathered in Fig. 8 and Table I. Generally, P depends neither on α , nor on the pump intensity, if recorded high enough above threshold (typically 20% higher). The results are quite reproducible, with error bars about 0.05, which means that the differences between shapes in Fig. 8 are relevant, and hence due to specific features of the lasing modes.

In square and pentagon, P is greater than zero, so I_{\parallel} component dominates. However P is significantly smaller than in a Fabry-Perot cavity, which evidences a redistribution of the light due to reflections at the borders. The difference between P_{square} and P_{pentagon} could arise from the periodic orbits sustaining the lasing modes, namely diamond orbit for square [see Figs. 3(b) and 3(c)] and pentagonal orbit for pentagon [26].

Eventually, the case of whispering gallery modes (WGM) should be considered. In stadium cavities [50], P is close to 1, as in Fabry-Perot lasers, whereas spectral analysis confirms that the lasing modes are indeed WGM [2]. Actually stadium shape leads to chaotic dynamical systems, which could result in a short photon lifetime (~ 1 ps)⁵ and then to a lasing behavior close to the Fabry-Perot cavity. With stadiums, we did not

⁵The photon lifetime of stadiums can be estimated from passive simulations. In [2] Fig. 23(a), the simulation corresponds to the same shape ratio than the experiments presented here. The imaginary part of the wave number [$\text{Im}(kR)$] of the most confined modes seems to be almost constant versus the real part of the wave number. The photon lifetime can then be estimated from formula $\tau \sim \frac{1}{c \cdot \text{Im}(k)}$, with c as a speed of light in vacuum, $\text{Im}(kR) \sim 0.15$ from simulations, and $R = 60 \mu\text{m}$ in experiments, which leads to $\tau \sim 1$ ps.

notice any influence on P neither of the pump polarization α , nor of the cavity aspect ratio (ratio between length and radius; see [2], for instance).

Disk should be the archetypal shape for WGM. However, the presence of the substrate hinders their observation [51]. The P values reported here were then measured from disks lying on a pedestal. As reported in [51], these cavities present two kinds of lasing mode families: WGM and Fabry-Perot-like modes. The latter behave like real Fabry-Perot modes, in particular, regarding their P value. On the contrary, WGM are insensitive to the pump polarization α and their P value is close to zero, probably thanks to a long photon lifetime,⁶ which allows for an efficient mixing of the polarized components at the boundary [3].

Finally we considered kite-shaped micro-lasers,⁷ which are defined by a slight deformation from a disk [53] and present the crucial advantage to emit WGM without requiring a pedestal technology. In that case, P is negative. The structure of the electromagnetic modes is then allowing by itself to flip the ratio between the polarized components, which was forced by the gain properties in the other shapes.

In order to improve the understanding of the mode structure and the monitoring of the emitted polarization, it would be interesting to release the prevalence of TE polarization due to the gain material. As shown in Table I, the use of another laser dye does not significantly alter the TE prevalence. Actually theoretical curves in Fig. 4 indicate that the angle β between the absorption and emission dipoles should be greater than 55° to expect a negative P . As β is usually small for S_0 - S_1 transitions, a drastic change cannot be expected that way. To significantly improve I_\perp supplies, two different experimental schemes are considered and implemented in the following sections.

VI. USE OF RESONANT ENERGY TRANSFER

An obvious method to promote the I_\perp component would be to use a dye with a molecular structure capable of isotropically redistributing the pump excitation. For this purpose, the small organo-metallic molecule Alq₃ is a good candidate, thanks to its symmetrical propeller shape. Unfortunately, Alq₃ cannot be used as a gain material alone, as in spite of being fluorescent, to our knowledge, no stimulated emission has been reported to date. But it is possible to add a laser dye, which will provide stimulated emission after a transfer of excitation via Alq₃

⁶For a perfect two-dimensional disk, the quality factor is huge for the parameter kR , which is used in our experiments ($kR \sim 1000$). It is then difficult to estimate it from numerical calculations. From simulations, it seems that the quality factor of the best confined modes is growing logarithmically versus $\text{Re}(kR)$: $\log_{10} Q \sim 0.25\text{Re}(kR)$. The extrapolation to $k = 2\pi/0.6 \mu\text{m}^{-1}$ and $R = 100 \mu\text{m}$ leads then to $Q \sim 10^{250}$, and so to a photon lifetime $\tau = Q/ck \sim 10^{235}$ s. Anyway, this photon lifetime is highly shortened by several processes, such as wall roughness or diffraction at the boundary, and the highest reported quality factors are about 10^{10} (see a review in [52]). In our experiments, we expect that the nanometric quality etching ensures a photon lifetime greater than 10–100 ps.

⁷The boundary is defined by the polar equation $\rho(t) = \rho_0(\cos t - 2d \sin^2 t)$, with $d = 0.165$ in this paper.

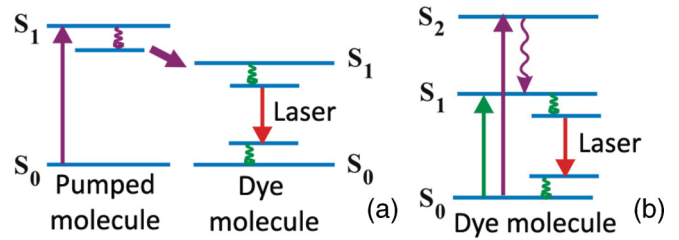


FIG. 9. (Color online) Pumping schemes are (a) via energy transfer from an excited molecule to the laser dye, (b) direct pumping to the S_2 state of the dye laser.

[54,55]. The scheme of the experiment is presented in Fig. 9(a). We expect an emission in both polarizations due to RET and the specific Alq₃ geometry.

For this experiment, we used a pulsed frequency-tripled Nd:YAG laser (355 nm, 300 ps, 10 Hz) to excite the Alq₃ molecule in its $S_0 \rightarrow S_1$ absorption band. For the purity of the demonstration, the required laser dye should have negligible absorption at the pumping wavelength (355 nm) to ensure that the emission results from energy transfer. Besides, to provide an efficient energy transfer, the fluorescence spectrum of Alq₃ should significantly overlap with the absorption band of the laser dye. RH590 verifies both criteria as shown in Fig. 10.

3. Planar microlasers

Alq₃ and RH590 were taken in quantities necessary to satisfy a 1:1 stoichiometric ratio for 5% wt of RH590 in PMMA. The fluorescence emission of RH590-Alq₃ under 355-nm pumping was 10 times more intense than for RH590 alone [see Fig. 10(b)], which confirms the presence of an efficient energy transfer. In the case of ASE, the degree of polarization P for RH590 under 532-nm pumping is 0.5, while introducing Alq₃ molecules it decreases to -0.1 under 355-nm pumping. For RH590 alone under 355-nm pumping, there was even no measurable ASE signal. The transfer of excitation via Alq₃ is then an efficient method to increase the participation of I_\perp . However, the consequences on lasing could not be checked

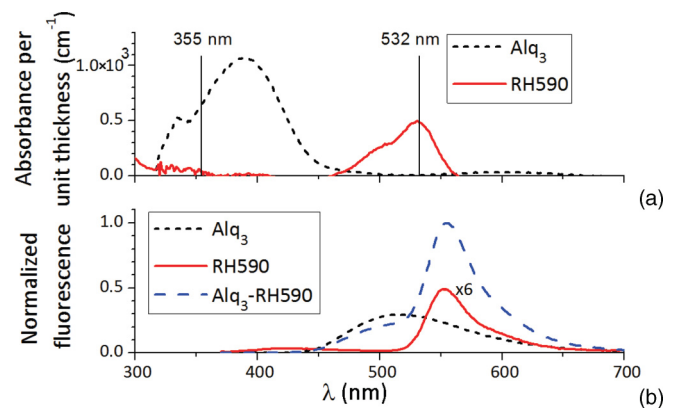


FIG. 10. (Color online) (a) Absorption spectra of Alq₃ and RH590. (b) Fluorescence spectra of Alq₃, RH590 and Alq₃-RH590 under the same pump intensity at 355 nm. They are normalized by the maximum of Alq₃-RH590 fluorescence spectrum and the variation of layer thickness is taken into account.

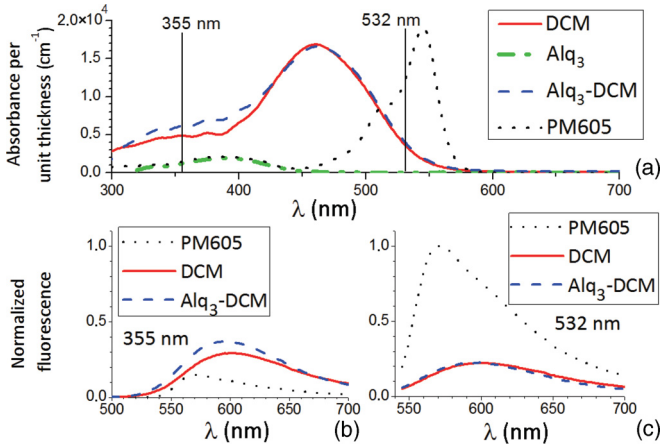


FIG. 11. (Color online) (a) Absorption spectra of PM605, DCM, Alq₃, and Alq₃-DCM. (b) and (c) Fluorescence spectra of PM605, DCM, and Alq₃-DCM under pumping at wavelengths of 355 nm (b) and 532 nm (c), normalized by the maximum of PM605 fluorescence spectrum under 532-nm pumping wavelength.

since no lasing from RH590-Alq₃ was observed, probably due to low gain values.

Similar experiments were then performed with DCM, since the transfer in Alq₃-DCM is known to be very efficient [56]. The perpendicular component of the electric field shows indeed higher intensities under lasing in various resonator shapes of in-plane microlasers. The P values are summarized in Table I. However, it is difficult to say if the decreasing of P can be only assigned to RET via Alq₃, since DCM absorbs significantly at 355 nm [see Fig. 11(a)]. Actually we show in the next section that absorption to higher excited states can be used to modify the P values.

VII. ABSORPTION IN HIGHER EXCITED STATES

To reach small or negative P values—which corresponds to the involvement of TM polarized modes—Fig. 4 shows that the angle β between the absorption and emission transition dipoles must be large. However, using the $S_0 \rightarrow S_1$ transition only, β is usually small. To release this constraint, a second method is based on pumping the dye laser to higher excited states. Actually the absorption dipole of a dye molecule is in general oriented in a very different manner for $S_0 \rightarrow S_n$ ($n > 1$). For illustration, the absorption dipoles for $S_0 \rightarrow S_1$ and $S_0 \rightarrow S_2$ of DCM, PM605, and MD7 were calculated with GAUSSIAN software and reported in Fig. 2. After absorption, it is expected that the molecule relaxes from the S_2 state to the S_1 state, and then emits, as depicted in Fig. 9(b). For DCM, PM605, and MD7 some β angle between $\vec{d}_a(0 \rightarrow 2)$ and $\vec{d}_e(1 \rightarrow 0)$ are close to $\pi/2$, and negative P values are thus expected, as predicted in Fig. 4 and reported in [43]. Figure 11(b) confirms that DCM and PM605 can indeed be pumped within a higher excited state and then emit from the S_1 state. It is, however, difficult to single out which specific state of the dye lasers is being excited, since the absorption curves of the transitions partially overlap.

Contrary to the case of Sec. IV and in accordance with the expectations, ASE under 355-nm pumping switches to smaller

or negative P values: $P_{\text{DCM},355} = 0.1$ and $P_{\text{PM605},355} = -0.50$ (planar configuration).

4. VECOLS

In VECOL configuration, the experiment of Sec. V was again carried out, inserting a glass plate inside the cavity at Brewster angle to force the emission polarization, and then turning the polarization of the pump beam by an angle α' . The results for a DCM-PMMA layer are plotted with circles in Fig. 7. Contrary to the case of 532-nm pumping, under a high 355-nm pumping, the laser emission is now almost insensitive to the pump polarization, which corresponds to $P = 0$. Besides, we performed time-resolved measurements of fluorescence anisotropy [57] and got $P \sim 0$ under a 355-nm pumping, even at very short delay after excitation. This effect could be assigned to different absorbing transitions, or maybe to RET occurring during the S_n to S_1 nonradiative transitions.

5. Planar microlasers

In microlaser configuration, pumping into higher excited states is also an efficient way to modify significantly the ratio between polarized components. Results for DCM and PM605 are summarized in Table I. However, the cavities suffered from a considerable bleaching, whereas it was not even an issue under the $S_0 \rightarrow S_1$ pumping. For reliable results, we then used a homemade laser dye, called MD7 [24], for which molecular structure and absorption dipole moments are presented in Fig. 2. The degree of polarization P was plotted in Fig. 8 for various cavity shapes and shows indeed considerably lower values than under 532-nm pumping. An important point is that P is still positive for ASE, while it is clearly negative for diamond modes in a square microlaser, and for WGM in a kite microlaser. So, although TE polarization is favored due to gain material and/or propagation, the coupling to TM modes within the resonator is strong enough to reverse the balance in favor of I_{\perp} .

To summarize, with a robust laser dye, pumping into high excited states is indeed an appropriate way to get a lasing polarization which is not strictly constrained by the pump polarization and pump geometry.

VIII. CONCLUSION

In this paper, we investigated the polarization states of organic solid-state lasers in two different configurations, VECOL and in-plane microresonators. The framework of fluorescence anisotropy was used to interpret the data and showed that pump geometry favors a specific component of the electric field: parallel to the pump polarization for VECOL and in-plane for microlasers. To release this constraint, we demonstrated that pumping into higher excited states of the laser dye can modify significantly the ratio between the polarized components of the emitted field. These experiments were used to explore the influence of the resonator shape on the polarization states. For Fabry-Perot cavities, thanks to the feedback, there is an enhancement of the dominant polarization compared to amplified spontaneous emission. On the contrary, for resonances with long photon lifetimes, like WGM, the polarization states can be strongly modified by coupling of

the electromagnetic components at the cavity boundary. This opens the way to a more systematic investigation of the relationship between mode structure and resonator shape, by combining experimental setup [58] and numerical simulations which should be both able to capture the three-dimensional nature of the electromagnetic field.

ACKNOWLEDGMENTS

The authors acknowledge J. Delaire, S. Brasselet, H. Benisty, and S. Bittner for fruitful discussions, A. Nosich and E. Smotrova for suggesting kite-shaped cavities, and I. Ledoux-Rak for financial support.

APPENDIX A: DIPOLAR MOMENTS

The absorption transition dipole from the fundamental state f to an excited state e is defined as the following vector (see p. 434 of Ref. [59]):

$$\vec{d}_a(f \rightarrow e) = \langle \psi_f | \hat{d} | \psi_e \rangle, \quad (\text{A1})$$

where ψ_f and ψ_e are the stationary wave functions of the involved states, and \hat{d} is a vector operator that is the sum of the position vectors of all charged particles weighted with their charge. Absorption is a fast process; the positions of the nucleus are thus assumed to be fixed, and only the electronic part of the wave functions changes between ψ_f and ψ_e . Laser dyes are often plane aromatic molecules and the $S_0 \rightarrow S_1$ transition corresponds to the transfer of a single electron from a π to a π^* orbital. These orbitals are both symmetrical above and below the plane of the molecule, and so the integral (A1) along the direction perpendicular to this plane is zero, since the global function to integrate is odd. Hence $\vec{d}_a(0 \rightarrow 1)$ lies in the plane of the molecule. If the dye is pumped in its S_2 state, the excited wave function involves in general a π^* orbital as well, and $\vec{d}_a(0 \rightarrow 2)$ remains in the plane of the molecule. However, the profile of the π^* orbitals in the plane are different, and thus their corresponding \vec{d}_a are not oriented similarly.

The definition of the emission transition dipole is similar to (A1), except the expression of ψ_e . Usually the molecule relaxes before emitting and the wave function of the excited state should then take into account the vibrations of the nucleus. Strictly speaking, the emission dipole is hence different from the absorption dipole of the same transition. However, the rearrangement in the S_1 state is in general not very huge and the angle β between the dipoles \vec{d}_a and \vec{d}_e remains close to zero.

Absorption dipoles were calculated with GAUSSIAN software and reported in Fig. 2. $S_0 \rightarrow S_1$ transition moments are calculated to be (4.04; 0.45; 0) for DCM, (0.3; -3.1; 0) for MD7 and (2.41; 1.35; 0.17) for PM605, while $S_0 \rightarrow S_2$ is (-0.8; -1.27; 0) for DCM, (-1.53; -0.02; -0) for MD7, and (-1.06; -0.6; -0.11) and (0.28; -0.54; 0.2) for PM605. The coordinates correspond to a frame, which is specific to each molecule and is indicated in Fig. 2.

APPENDIX B: DEGREE OF POLARIZATION

In this appendix, we derive formulas (1) and (2) in a similar way to those in [19] and [20], but adapted to the specific

geometry of the devices in Fig. 1. Here we assume that the fluorophores are isotropically distributed in a bulk material and unable to rotate. The case of an anisotropic distribution is dealt with in [38].

The dye molecules are excited by a linearly polarized electric field defined by a unit vector $\mathbf{e} = \{\sin \alpha, \cos \alpha, 0\}$. A single molecule from the ensemble is located from its emission transition dipole \vec{d}_e with the usual spherical coordinates $\Omega = (\theta, \varphi)$. The orientations of its transition dipoles are then characterized by the following unit vectors,

$$\begin{aligned} \mathbf{u}_a &= \frac{\vec{d}_a}{\|\vec{d}_a\|} \\ &= \{\sin \theta_a \cos(\varphi + \psi), \sin \theta_a \sin(\varphi + \psi), \cos \theta_a\}, \end{aligned}$$

for absorption and

$$\mathbf{u}_e = \frac{\vec{d}_e}{\|\vec{d}_e\|} = \{\sin \theta \cos \varphi, \sin \theta \sin \varphi, \cos \theta\},$$

for emission. The notations are summarized in Fig. 12.

We are interested in the emission along axis z for a VEC-SOL configuration and along axis y for in-plane resonators. In the far-field approximation, the intensity emitted along a given axis j (z or y) can be presented as a three-dimensional integral of the following product: absorption probability $P_a \propto (\mathbf{e} \cdot \mathbf{u}_a)^2$ and Poynting vector $\Pi_{e j}(\theta, \varphi) \propto (\mathbf{j} \times \mathbf{u}_e)^2$ integrated over all possible orientations Ω of the emission dipoles and ψ of the absorption dipole around the emission dipole:

$$I_j = I_{j0} \int_{\Omega} P_a(\Omega) \Pi_{e j}(\Omega) d\Omega. \quad (\text{B1})$$

The modulus squared of the Poynting vector can always be presented as a sum of two orthogonal polarizations:

$$\begin{aligned} \Pi_{e y}(\Omega) &\propto \underbrace{\cos^2 \theta}_{I_{\parallel}} + \underbrace{\sin^2 \theta \cos^2 \varphi}_{I_{\perp}}, \\ \Pi_{e z}(\Omega) &\propto \underbrace{\sin^2 \theta \sin^2(\varphi + \alpha)}_{I_{\parallel}} + \underbrace{\sin^2 \theta \cos^2(\varphi + \alpha)}_{I_{\perp}}, \end{aligned}$$

where I_{\parallel} and I_{\perp} are defined in Fig. 1. After integration over all the possible orientations of the absorption moment around

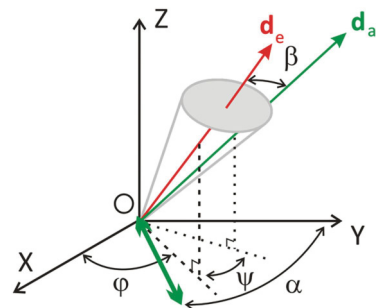


FIG. 12. (Color online) Notations are as follows: absorption (\vec{d}_a) and emission (\vec{d}_e) transition dipoles are oriented at the angles θ_a and θ_e with respect to the z axis, β , angle between the moments, ψ , between their projections on the xy plane, φ , angle between the x axis and projection of \vec{d}_e on the xy plane, α , angle between the y axis and the pump beam polarization (thick green arrow).

the emission one, we get the following expression for the probability of absorption⁸:

$$P_a(\Omega) \propto 2 - 2 \cos^2 \beta - (1 - 3 \cos^2 \beta) \sin^2 \theta \times [1 - \cos(2\varphi + 2\alpha)]. \quad (\text{B2})$$

Then integration over Ω must be performed and leads to intensity components of interest:

$$I_{\parallel \text{ in plane}} \propto \frac{1}{30} [3 + \cos^2 \beta + \cos 2\alpha(1 - 3 \cos^2 \beta)], \quad (\text{B3})$$

$$\begin{aligned} I_{\perp \text{ in plane}} &= I_{\parallel \text{ in plane}}(\alpha = 0), \\ I_{\parallel \text{ VECSOL}} &= I_{\parallel \text{ in plane}}(\alpha = \pi/2), \\ I_{\perp \text{ VECSOL}} &= I_{\perp \text{ in plane}}. \end{aligned} \quad (\text{B4})$$

Therefore the expressions for the degrees of polarization P are

$$P_{\text{in plane}} = \frac{(3 \cos^2 \beta - 1)(1 - \cos 2\alpha)}{7 - \cos^2 \beta - \cos 2\alpha(3 \cos^2 \beta - 1)}, \quad (\text{B5})$$

$$P_{\text{VECSOL}} = \frac{3 \cos^2 \beta - 1}{3 + \cos^2 \beta}. \quad (\text{B6})$$

From these expressions, it follows that for a pump beam polarization characterized by $\alpha = \pi/2$ (orthogonal to the direction of observation), then $P_{\text{in plane}} = P_{\text{VECSOL}}$. The variation of $P_{\text{in plane}}$ with β angle is depicted on Fig. 4 for several orientations α of the linear pump polarization.

⁸Error in Eq. (6) of [38]. It should be read $\cos 2\varphi \cos 2\alpha$ instead of $\cos(2\varphi + 2\alpha)$

-
- [1] H. E. Tureci, A. D. Stone, and L. Ge, *Phys. Rev. A* **76**, 013813 (2007).
- [2] E. Bogomolny, N. Djellali, R. Dubertrand, I. Gozhyk, M. Lebental, C. Schmit, C. Ulysse, and J. Zyss, *Phys. Rev. E* **83**, 036208 (2011).
- [3] N. Frateschi, A. Kanjamala, A. F. J. Levi, and T. Tanbun-Ek, *Appl. Phys. Lett.* **66**, 1859 (1995).
- [4] D. K. Kim, S.-J. An, E. G. Lee, and O'Dae Kwon, *J. Appl. Phys.* **102**, 053104 (2007).
- [5] N. Tsujimoto, T. Takashima, T. Nakao, K. Masuyama, A. Fujii, and M. Ozaki, *J. Phys. D: Appl. Phys.* **40**, 1669 (2007).
- [6] S. V. Frolov, M. Shkunov, Z. V. Vardeny, and K. Yoshino, *Phys. Rev. B* **56**, 4363R (1997).
- [7] J. Wang and K. Y. Wong, *Appl. Phys. B* **87**, 685 (2007).
- [8] Chao Ye, Lei Shi, Jun Wang, Dennis Lo, and Xiao-lei Zhu, *Appl. Phys. Lett.* **83**, 4101 (2003).
- [9] H. Rabbani-Haghighi, S. Forget, S. Chénais, and A. Siove, *Opt. Lett.* **35**, 1968 (2010).
- [10] A. Matsko, editor, *Practical Applications of Micro-Resonators in Optics and Photonics* (CRC, Boca Raton, 2009).
- [11] Lu Ding, C. Baker, P. Senellart, A. Lemaitre, S. Ducci, G. Leo, and I. Favero, *Phys. Rev. Lett.* **105**, 263903 (2010).
- [12] P. Del'Haye, T. Herr, E. Gavartin, M. L. Gorodetsky, R. Holzwarth, and T. J. Kippenberg, *Phys. Rev. Lett.* **107**, 063901 (2011).
- [13] N. Djellali, I. Gozhyk, D. Owens, S. Lozenko, M. Lebental, J. Lautru, C. Ulysse, B. Kippelen, and J. Zyss, *Appl. Phys. Lett.* **95**, 101108 (2009).
- [14] Q. J. Wang, C. Yan, N. Yu, J. Unterhinninghofen, J. Wiersig, C. Pflügl, L. Diehl, T. Edamura, M. Yamanishi, H. Kan, and F. Capasso, *PNAS* **107**, 22407 (2010).
- [15] C. Li and A. W. Poon, *Opt. Lett.* **30**, 546 (2005).
- [16] See Sec. III. B.2 in [2].
- [17] J. Topolancik and F. Vollmer, *Biophys. J.* **92**, 2223 (2007).
- [18] S. Chénais and S. Forget, *Polym. Int.* **61**, 390 (2012).
- [19] J. R. Lakowicz, *Principles of Fluorescence Spectroscopy*, 3rd ed. (Springer, New York, 2006).
- [20] B. Valeur, *Molecular Fluorescence: Principles and Applications* (Wiley-VCH, New York, 2001).
- [21] K. C. Reyzer and L. W. Casperson, *J. Appl. Phys.* **51**, 6075 (1980).
- [22] K. C. Reyzer and L. W. Casperson, *J. Appl. Phys.* **51**, 6083 (1980).
- [23] O. I. Yaroshenko, *J. Opt. A: Pure Appl. Opt.* **5**, 328 (2003).
- [24] E. Y. Schmidt, N. V. Zorina, M. Y. Dvorko, N. I. Protsuk, K. V. Belyaeva, G. Clavier, R. Méallet-Renault, T. T. Vu, A. B. I. Mikhaleva, and B. A. Trofimov, *Chem. Eur. J.* **17**, 3069 (2011).
- [25] M. Lebental, E. Bogomolny, and J. Zyss, Organic micro-lasers: a new avenue onto wave chaos physics, in [10].
- [26] M. Lebental, N. Djellali, C. Arnaud, J.-S. Lauret, J. Zyss, R. Dubertrand, C. Schmit, and E. Bogomolny, *Phys. Rev. A* **76**, 023830 (2007).
- [27] G. Dutier, V. de Beaucoudrey, A. C. Mitus, and S. Brasselet, *Eur. Phys. Lett.* **84**, 67005 (2008).
- [28] G. Dutier, V. de Beaucoudrey, S. Brasselet, and J. Zyss (unpublished).
- [29] V. Le Floc'h, S. Brasselet, J.-F. Roch, and J. Zyss, *J. Phys. Chem. B* **107**, 12403 (2003).
- [30] V. Bulović, V. G. Kozlov, V. B. Khalfin, and S. R. Forrest, *Science* **279**, 553 (1998).
- [31] I. Gozhyk *et al.* (in preparation).
- [32] O. Svelto, *Principles of Lasers* (Plenum Press, New York, 1998).
- [33] E. W. Thulstrup and J. Michl, *J. Am. Chem. Soc.* **104**, 5594 (1982).
- [34] M. Tammer and A. P. Monkman, *Adv. Mat.* **14**, 210 (2002); C. M. Ramsdale and N. C. Greenham, *ibid.* **14**, 212 (2002).
- [35] J. Sturm, S. Tasch, A. Niko, G. Leising, E. Toussaere, J. Zyss, T. C. Kowalczyk, K. D. Singer, U. Scherf, and J. Huber, *Thin Solid Films* **298**, 138 (1997).
- [36] S. Agan, F. Ay, A. Kocabas, and A. Aydinli, *Appl. Phys. A* **80**, 341 (2005).
- [37] L. Novotny, M. R. Beversluis, K. S. Youngworth, and T. G. Brown, *Phys. Rev. Lett.* **86**, 5251 (2001).
- [38] I. Gozhyk, S. Forget, S. Chénais, C. Ulysse, A. Brosseau, R. Méallet-Renault, G. Clavier, R. Pansu, J. Zyss, and M. Lebental, *Proceedings of SPIE* **8258**, 82580K (2012).
- [39] S. Y. Lam and M. J. Damzen, *Appl. Phys. B* **77**, 577 (2003).
- [40] T. D. Visser, B. Demeulenaere, J. Haes, D. Lenstra, R. Baets, and H. Blok, *J. Lightwave Technol.* **14**, 885 (1996).

- [41] S. Bittner, B. Dietz, M. Miski-Oglu, P. O. Iriarte, A. Richter, and F. Schafer, *Phys. Rev. A* **80**, 023825 (2009).
- [42] B. B. McFarland, *Appl. Phys. Lett.* **10**, 208 (1967).
- [43] I. Nagata and T. Nakaya, *J. Phys. D: Appl. Phys.* **6**, 1870 (1973).
- [44] X. Wang, R. A. Linke, G. Devlin, and H. Yokoyama, *Phys. Rev. A* **47**, 2488R (1993).
- [45] L. Persano, P. del Carro, E. Mele, R. Cingolani, D. Pisignano, M. Zavelani-Rossi, S. Longhi, and G. Lanzani, *Appl. Phys. Lett.* **88**, 121110 (2006).
- [46] S. A. van den Berg, V. A. Sautenkov, G. W. 't Hooft, and E. R. Eliel, *Phys. Rev. A* **65**, 053821 (2002).
- [47] A. Aiello, F. de Martini, and P. Mataloni, *Opt. Lett.* **21**, 149 (1996).
- [48] H. Rabbani-Haghighi, S. Forget, A. Siove, and S. Chénais, *Eur. Phys. J. Appl. Phys.* **56**, 34108 (2011).
- [49] T. Ikegami, *IEEE J. Quantum Electron.* **8**, 470 (1972).
- [50] M. Leubenthal, J.-S. Lauret, J. Zyss, C. Schmit, and E. Bogomolny, *Phys. Rev. A* **75**, 033806 (2007).
- [51] S. Lozenko, N. Djellali, I. Gozhyk, C. Delezoide, J. Lautru, C. Ulysse, J. Zyss, and M. Leubenthal, *J. Appl. Phys.* **111**, 103116 (2012).
- [52] K. J. Vahala, *Nature (London)* **424**, 839 (2003).
- [53] M. V. Balaban, E. I. Smotrova, O. V. Shapoval, V. S. Bulygin, A. I. Nosich, *Int. J. Numerical Modeling: Electronic Networks, Devices and Fields* **25**, 490 (2012).
- [54] M. Berggren, A. Dodabalapur, R. E. Slusher, and Z. Bao, *Nature (London)* **389**, 466 (1997).
- [55] V. G. Kozlov, V. Bulović, P. E. Burrows, and S. R. Forrest, *Nature (London)* **389**, 362 (1997).
- [56] V. G. Kozlov, V. Bulović, P. E. Burrows, M. Baldo, V. B. Khalfin, G. Parthasarathy, S. R. Forrest, Y. You, and M. E. Thompson, *J. Appl. Phys.* **84**, 4096 (1998).
- [57] J.-A. Spitz, R. Yasukuni, N. Sandeau, M. Takano, J.-J. Vachon, R. Méallet-Renault, and R. B. Pansu, *J. Microscopy-Oxford* **229**, 104 (2008).
- [58] D. K. Kim, S.-J. An, E. G. Lee, and O'Dae Kwon, *J. Appl. Phys.* **102**, 053104 (2007).
- [59] E. Braslavsky, *Pure Appl. Chem* **79**, 293 (2007).